A new semiconductor: Ti_{0.5}Mg_{0.5}N(001)

Baiwei Wang and Daniel Gall*
Department of Materials Science and Engineering
Rensselaer Polytechnic Institute
Troy, NY 12180, USA
*galld@rpi.edu

Abstract—Ti_{0.5}Mg_{0.5}N has recently been predicted to be a semiconductor with a 1.3 eV band gap and promising properties for thermoelectric and plasmonic devices. As a first step towards experimental validation, epitaxial Ti_{0.5}Mg_{0.5}N(001) layers are deposited on MgO(001) by reactive magnetron co-sputtering from titanium and magnesium targets at 600 °C in pure N₂ atmospheres. X-ray diffraction ω -2 θ scans, ω -rocking curves, φ scans, and high resolution reciprocal space maps show that Ti_{0.5}Mg_{0.5}N alloys form a pseudobinary rocksalt structure and are single crystals with a cube-on-cube epitaxial relationship with the substrate: $(001)_{\text{TiMgN}} \| (001)_{\text{MgO}}$ and $[100]_{\text{TiMgN}} \| [100]_{\text{MgO}}$. A 275-nm-thick Ti_{0.5}Mg_{0.5}N layer is fully relaxed and exhibits a 002 ω -rocking curve width $\Gamma_{\omega} = 0.73^{\circ}$, while a 36-nm-thick layer is fully strained and has a $\Gamma_{\omega} = 0.49^{\circ}$. These results indicate a thickness-dependent strain state which suggests a critical thickness for misfit dislocation nucleation and glide which is between 36 and 275 nm. A measured negative temperature coefficient of resistivity in combination with a low optical absorption coefficient of 0.25×10^5 cm⁻¹ for $\lambda = 740$ nm, and a vanishing density of states at the Fermi level measured by x-ray photoelectron spectroscopy support the prediction that Ti_{0.5}Mg_{0.5}N is a semiconductor.

Keywords— TiMgN; semiconductor; ternary nitride; epitaxial

I. INTRODUCTION

TiN is well known for its high hardness, wear and corrosion resistance, and high temperature stability and is used in hard wear-protective coatings, diffusion barriers, and optical or decorative coatings [1-7]. In addition, TiN is also promising as a gate electrode material [6] and as a conductor for plasmonics [8-10]. Alloying of TiN with nitrides of elements with more or less valence electrons can be effectively used to control the density of conduction electrons [11-14]. Here, we investigate a promising option of alloying TiN with the alkaline earth element Mg. This has the potential to extend the opportunities for controlling the carrier density, as simple electron counting suggests that a 50-50 Ti-to-Mg ratio leads to a vanishing carrier density, while x < 0.5 and x > 0.5correspondingly would result in n and p-type electron transport in Ti_{1-x}Mg_xN, respectively [9, 15, 16]. The Ti_{1-x}Mg_xN alloy is relatively unexplored. A few investigations show that the incorporation of Mg in TiN changes the color [17], increases wear and oxidation resistance [18], yields a tunable infrared plasmonic activity [9, 19] and may become useful as a plasmonic solar heat transducer [20]. First-principles studies predict the phase stability of TiMgN₂ [21] and an ordered TiMgN₂ phase as well as a B1-structure Ti_{0.5}Mg_{0.5}N solid solution are semiconductors with band gaps of 1.1 and 1.3 eV, respectively, as determined using hybrid functional calculations [22]. A more recent study which uses the conventional generalized gradient approximation (GGA) reports a much smaller indirect gap of 0.27 eV for TiMgN₂ [23], which can be attributed to the typical underestimation of bandgaps by the GGA. In summary, Ti_{0.5}Mg_{0.5}N is predicted to be a semiconductor while simultaneously also exhibiting promising mechanical and corrosion-protective properties. This motivates our study on the growth and electronic properties of epitaxial Ti_{0.5}Mg_{0.5}N(001) layers, with the goal to validate that Ti_{0.5}Mg_{0.5}N is a semiconductor.

II. EXPERIMENTAL PROCEDURE

Ti_{0.5}Mg_{0.5}N layers were deposited on single-crystal MgO(001) substrates by reactive magnetron co-sputtering at 600 °C in pure N₂ atmospheres using a load-locked ultra-high vacuum deposition system with a base pressure of 10⁻⁹ Torr, which is described in more detail in [16]. The power to the 99.99% pure Ti and Mg targets p_{Ti} and p_{Mg} were adjusted to achieve a one-to-one ratio between Ti and Mg in the deposited alloys. The results in this paper are primarily from two samples: the first is a $Ti_{0.5}Mg_{0.5}N$ layer with thickness d = 36nm, deposited with $p_{Ti} = 100$ W, $p_{Mg} = 350$ W, and a N_2 pressure $P_{N2} = 5$ mTorr, while the corresponding parameters for the 2nd $Ti_{0.5}Mg_{0.5}N$ layer are d = 275 nm, $p_{Ti} = 100$ W, p_{Mg} = 20 W, $P_{\rm N2}$ = 15 mTorr. The different required $p_{\rm Ti}/p_{\rm Mg}$ ratios to achieve a 1:1 ratio of Ti and Mg for these two samples was primarily due to the different chosen target-to-substrate distances (9 vs 23 cm) during deposition. The compositions were analyzed by x-ray photoelectron spectroscopy (XPS) acquired using Al K_α radiation (1486.7 eV) in a PHI 5000 VersaprobeTM system calibrated using the C 1s peak at 284.8 eV from absorbed surface carbon, yielding Ti/Mg = $1.02 \pm$ 0.02 and 0.97 ± 0.02 for the two layers. Rutherford Backscattering Spectroscopy with 2 MeV 4He+ ions was used to confirm the XPS results, indicating agreement within 0.04 for the measured Ti-to-Mg ratio. Valence-band spectra were acquired using the same XPS system, operated with a 23.5 eV pass energy and a 0.2 eV step size over the binding energy range $E_{\rm b}$ = -2 to 20 eV. The as-deposited and air-exposed samples were not sputter cleaned in the XPS system, since the atomic ratio, especially N-to-metal ratio, is expected to be affected by preferential sputtering during surface cleaning [24]. We have chosen x-rays rather than ultraviolet radiation to acquire the valence band spectra despite the smaller energy resolution and signal-to-noise ratio, because the larger x-ray photoelectron escape depth results in a smaller sensitivity to surface contamination and defects.

X-ray diffraction was done with a Panalytical X'Pert PRO MPD system with a Cu K_{α} source. A two-bounce two-crystal Ge(220) monochromator was used, yielding a parallel incident beam with a wavelength of $\lambda_{K\alpha l} = 1.5406$ Å. ω -2 θ scans and ω rocking curves were obtained using a PIXcel solid-state line detector in receiving mode with 3 active channels. Asymmetric high-resolution reciprocal space maps (HR-RSM) around 113 reflections were obtained using the line detector in scanning mode, yielding fast high-resolution mapping by narrowing the beam using a relatively small angle (10-14°) between the sample surface and the detector to increase the 2θ resolution. φ scans from 111 reflections were acquired using a point focus xray lens (poly-capillary optics) that provides a quasi-parallel Cu K_{α} beam with a divergence of less than 0.3° and therefore minimizes defocusing effects due to sample height variations. In addition, ω -2 θ scans with a divergent beam Bragg-Brentano geometry were done over a large 2θ range from 10-85° in order to detect small inclusions of possible secondary phases or misoriented grains.

III. RESULTS AND DISCUSSION

X-ray diffraction ω -2 θ scans from the Ti_{0.5}Mg_{0.5}N layers deposited on MgO(001) exhibit only Ti_{0.5}Mg_{0.5}N 002 and MgO 002 peaks over the measured $2\theta = 10^{\circ}-85^{\circ}$ range, indicating preferred 001 orientation. Fig. 1(a) shows a section of a ω -2 θ pattern, from a 36-nm-thick Ti_{0.5}Mg_{0.5}N layer. For clarity purposes, the intensity for $2\theta < 42.7^{\circ}$ is multiplied by 10^{2} , as labeled. Within the plotted $2\theta = 41.6^{\circ}-43.2^{\circ}$ range, two primary peaks are detected. The substrate 002 reflection at 2θ = 42.91° corresponds to a MgO lattice constant $a_0 = 4.212$ Å, in agreement with the published literature value for bulk MgO crystals [25]. The less intense peak at 42.11° is from the 002 reflection from the Ti_{0.5}Mg_{0.5}N layer, yielding an out-of-plane lattice constant $a_{\perp} = 4.288$ Å. The a_{\perp} value agrees well with experimental data from Fenker et al (≤ 0.2%) [26] and Balzer et al ($\leq 0.1\%$) [17], but is slightly (-0.6%) smaller than the values predicted from first-principles calculations [22], which we attribute to the common overestimation of lattice constants by the generalized gradient approximation. We also note that the out-of-plane lattice constant is affected by the strain state of the layer, as discussed in detail below. The inset in Fig. 1(a) shows the ω rocking curve from the 002 reflection, which has a full-width at half-maximum (FWHM) of 0.49°, indicating strong crystalline alignment which suggests epitaxy. Fig. 1(b) shows an XRD φ -scan of the asymmetric 111 reflections from the same Ti_{0.5}Mg_{0.5}N layer. It is acquired using a 54.74° offset in χ and fixed $2\theta = 36.30^{\circ}$ and $\omega = 18.15^{\circ}$ to detect 111 reflections of the Ti_{0.5}Mg_{0.5}N layer by recording the reflected intensity as a function of the azimuthal angle φ . The plot shows four equally spaced peaks with an interval of 90°, labeled as 111, 111, 111, and 111. These are the four peaks that are expected for a cubic single crystal. Thus, the layer has a single in-plane orientation. The peaks occur at the same φ values as

for scans for which ω and 2θ are adjusted to detect the substrate MgO 111 reflections (not shown). This indicates, in combination with the results shown in Fig. 1(a), that the $Ti_{0.5}Mg_{0.5}N$ layer exhibits a cube-on-cube epitaxial relationship with the substrate: (001)TiMgN ||(001)MgO and [100]TiMgN ||[100]MgO.

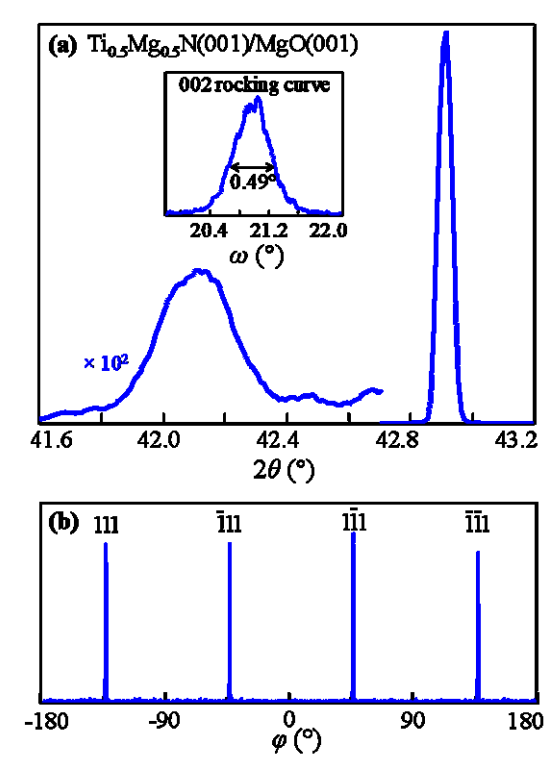


Fig. 1. X-ray diffraction (a) ω -2 θ scan of 002 reflections and (b) φ -scan of 111 reflections, from a 36-nm-thick epitaxial Ti_{0.5}Mg_{0.5}N(001) layer grown on MgO(001) in $P_{\rm N2}$ = 5 mTorr. Inset in (a) is the ω rocking curve of the 002 reflection.

Fig. 2 shows XRD high resolution RSMs acquired about asymmetric 113 reflections from the same 36-nm-thick Ti_{0.5}Mg_{0.5}N(001) layer (blue) as well as from an approximately 8 times thicker (275 nm) layer (red). The plot shows isointensity contour maps in a logarithmic scale, plotted within kspace where $k_{\perp} = 2\sin\theta\cos(\omega-\theta)/\lambda$ and $k_{\parallel} = 2\sin\theta\sin(\omega-\theta)/\lambda$ correspond to directions perpendicular and parallel to the substrate surface. Both maps show each two peaks: the 113 reflections from the MgO and Ti_{0.5}Mg_{0.5}N layers. The peak positions are used to determine the out-of-plane a_{\perp} and inplane a_{\parallel} lattice constants, which are $a_{\perp} = 3/k_{\perp} = 4.295 \pm 0.015$ Å and $a_{\parallel} = \sqrt{2} / k_{\parallel} = 4.211 \pm 0.005$ Å for the 36-nm-thick layer, and $a_{\perp} = 4.275 \pm 0.005$ Å and $a_{\parallel} = 4.268 \pm 0.005$ Å for the 275nm-thick layer. The a_{\perp} values agree well (~0.1% deviation) with 4.288 and 4.279 Å determined from ω -2 θ scans for the thin and thick layer, respectively. The relaxed lattice constant is obtained using $a_0 = (a_{\perp} - va_{\perp} + 2va_{\parallel}) / (1 + v)$, where v is the Poisson's ratio and is assumed to be 0.22±0.04, which is a typical value for titanium nitride [27, 28]. The relatively large estimated uncertainty in v has a negligible (0.07%) impact on the measured a_0 [29]. The resulting a_0 values from the two layers with thickness d = 36 and 275 nm are 4.265 ± 0.008 Å and 4.273 ± 0.006 Å, respectively. These values are identical

within the experimental uncertainty. In contrast, the two layers show considerable differences in the measured a_{\perp} and a_{\parallel} . More specifically, the 36-nm-thick $Ti_{0.5}Mg_{0.5}N$ layer exhibits a k_{\parallel} that is aligned with the substrate, as indicated by the vertical dashed line through the center of both peaks. This indicates that this layer has an a_{\parallel} that is matching the lattice constant of the MgO substrate. Thus, d = 36 nm leads to a Ti_{0.5}Mg_{0.5}N layer which is fully strained. In contrast, the peak from the 275-nm-thick layer is shifted with respect to the substrate peak such that the dashed line that connects the two peaks is parallel to the 113 ω - 2θ direction. This indicates that this layer is relaxed, consistent with the nearly identical a_{\perp} and a_{\parallel} values mentioned above. These results suggest that the total strain energy in the 36-nmthick layer is insufficient for noticeable relaxation while, in contrast, misfit dislocation nucleation and growth are substantial for the 275-nm-thick layer, leading to nearly perfect stress relaxation, which is attributed to the 7.6 times larger strain energy in the 7.6 times thicker layer. This is also consistent with the more pronounced broadening of the $Ti_{0.5}Mg_{0.5}N$ peak along the ω -direction for the thicker layer. Such broadening is primarily due to the crystalline mosaic spread and the misalignment of single crystal blocks, which is expected to increase with the presence of misfit dislocations and their associated non-uniform strain fields. We note here that the larger N₂ partial pressure used for the growth of the thicker layer may also play a minor role affecting the crystalline quality, based on the reported argument that a higher P_{N2} may lead to higher steady state N coverages and therefore lower cation surface mobilities and increased kinetic roughening during the growth of transition metal nitrides [27]. We also note that the broadening of the MgO 113 peak along the ω -direction is associated with small-angle grain boundaries in the single crystal substrates while the elongation from the top-left toward the bottom-right are intrinsic resolution streaks coming from the Ge(220) crystals in the hybrid monochromator [30].

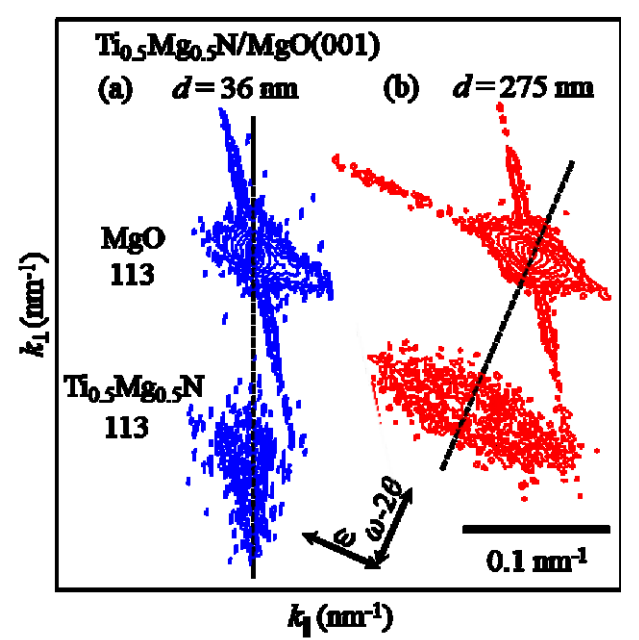


Fig. 2. HR-RSMs about asymmetric 113 reflections from $Ti_{0.5}Mg_{0.5}N(001)$ layers grown on MgO(001) with thickness (a) d = 36 nm and (b) d = 275 nm.

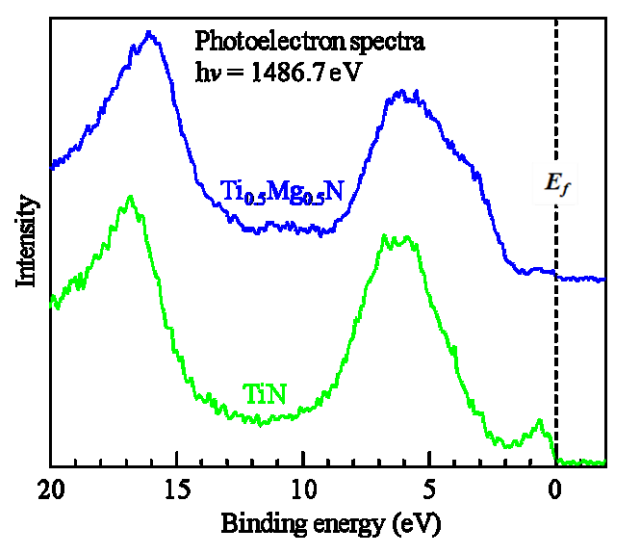


Fig. 3. XPS valence-band spectra from epitaxial $Ti_{0.5}Mg_{0.5}N(001)$ and TiN(001) layers.

An initial preliminary effort to experimentally confirm the prediction that Ti_{0.5}Mg_{0.5}N is a semiconductor is done using electron transport, optical, and density-of-states measurements. The measured room temperature resistivity of the d = 36 and 275 nm layers are 434 and 3197 $\mu\Omega$ ·cm, respectively. These values increase to 436 and 3636 $\mu\Omega$ ·cm for T = 77 K. That is, the temperature coefficient of resistivity (TCR) is slightly negative, consistent with Ti_{0.5}Mg_{0.5}N being a semiconductor. However, the negative TCR can also be explained by weak carrier localization as reported for other transition metal nitrides [12, 14, 31-35]. Optical transmission and reflection measurements provide values for the optical absorption coefficient at $\lambda = 740$ nm of 1.60×10^5 and 0.25×10^5 cm⁻¹ for the thin and thick layer, respectively. This relatively low absorption coefficient suggests the absence of direct interband transitions at this phonon energy [12, 36], also consistent with Ti_{0.5}Mg_{0.5}N being a semiconductor. However, this optical data does not rule out a lower energy in-direct gap or even band overlap, as previously shown for the similar rock-salt structure semiconductor ScN [37-39].

Fig. 3 shows an XPS valence-band spectrum from the 36nm-thick Ti_{0.5}Mg_{0.5}N(001) layer. For comparison, the plot also shows the measured spectrum from a pure TiN/MgO(001) layer grown at comparable deposition conditions as the Ti_{0.5}Mg_{0.5}N(001) layer. Based on previous computational [22, 40] and experimental [14, 36, 41] studies, the valence-band structures of transitional-metal (TM) nitrides exhibit three primary features associated with nitrogen 2s semicore states, hybridized N 2p-TM d states with e_g symmetry, and nonbonding TM d states with t_{2g} symmetry that define the conduction band. The TiN spectrum in Fig. 3 is in good agreement with previously reported spectra for TiN. [14, 42-44]. It exhibits the N 2s peak at 16.7 eV and the peak from the hybridized N 2p-Ti 3d states at 6.1 eV. The measured density of states (DOS) has a minimum at 2 eV below the Fermi level E_f , and then increases toward E_f which is associated with the non-bonding Ti 3d states. That is, the measured intensity in the TiN spectrum between 2 and 0 eV is from the TiN conduction band that contains one electron per formula unit and results in metallic conduction. We note that the decrease between 0.5 and 0.0 eV is due to experimental broadening, since the x-ray source yields only an approximately 1.0 eV resolution in the measured valence band spectrum. The Ti_{0.5}Mg_{0.5}N spectrum exhibits the N 2s peak at 16.1 eV and the hybridized N 2p-Ti/Mg 3d feature around 4 eV. However, there is no detectable DOS between 2 and 0 eV, suggesting that there are no electrons in the Ti/Mg 3d conduction band. A careful comparison to the TiN spectrum including a signal-to-noise analysis indicates that the measured intensity from Ti_{0.5}Mg_{0.5}N in this binding energy range is 10% of the intensity from TiN, but that this 10% signal also corresponds to the experimental noise level. Thus, the Ti_{0.5}Mg_{0.5}N conduction band has a measured electron density of 0.1±0.1 electrons per unit formula, consistent with Ti_{0.5}Mg_{0.5}N being a semiconductor. In addition, the right-shift of the N 2s and the hybridized N 2p-Ti/Mg 3d features in comparison to TiN suggest a decrease of E_f , from the conduction band to (possibly) the band gap, consistent with the overall electron counting argument and the fact that Ti_{0.5}Mg_{0.5}N is a semiconductor.

IV. CONCLUSIONS

For the purpose of experimentally validating that Ti_{0.5}Mg_{0.5}N is a semiconductor, epitaxial Ti_{0.5}Mg_{0.5}N(001) layers are deposited on MgO(001) by reactive magnetron cosputtering from titanium and magnesium targets at 600 °C in pure N_2 atmospheres. X-ray diffraction ω -2 θ scans, ω -rocking curves, φ -scans and high resolution reciprocal space maps show that Ti_{0.5}Mg_{0.5}N alloys form a pseudobinary rocksalt structure and are single crystals with a cube-on-cube epitaxial relationship with the substrate: (001)TiMgN | (001)MgO and [100]TiMgN | [100]MgO. A 36-nm-thick layer is coherent with the substrate while a 275-nm-thick Ti_{0.5}Mg_{0.5}N layer is fully relaxed, indicating a critical thickness for misfit dislocation nucleation and glide which is between 36 and 275 nm. A negative temperature coefficient of resistivity, a low optical absorption, and a negligible DOS at E_f measured by XPS valence-band spectroscopy support the prediction that $Ti_{0.5}Mg_{0.5}N$ is a semiconductor.

ACKNOWLEDGMENT

The authors acknowledge financial support by the National Science Foundation under Grant Nos. 1712752 and 1629230.

REFERENCES

- [1] J. E. Sundgren, "Structure and properties of TiN coatings," *Thin Solid Films*, vol. 128, pp. 21-44, June 1985.
- [2] H. Holleck, "Material selection for hard coatings," Journal of Vacuum Science & Technology A: Vacuum, Surfaces, and Films, vol. 4, pp. 2661-2669, 1986.
- [3] L. Hultman, "Thermal stability of nitride thin films," *Vacuum*, vol. 57, pp. 1-30, April 2000.
- [4] J. Musil, "Hard and superhard nanocomposite coatings," Surface and Coatings Technology, vol. 125, pp. 322-330, March 2000.
- [5] C.-S. Shin, D. Gall, N. Hellgren, J. Patscheider, I. Petrov, and J. E. Greene, "Vacancy hardening in single-crystal TiNx(001) layers," *Journal of Applied Physics*, vol. 93, pp. 6025-6028, 2003.

- [6] J. Westlinder, T. Schram, L. Pantisano, E. Cartier, A. Kerber, G. S. Lujan, J. Olsson, and G. Groeseneken, "On the thermal stability of atomic layer deposited TiN as gate electrode in MOS devices," *IEEE Electron Device Letters*, vol. 24, pp. 550-552, 2003.
- [7] J. S. Chawla, X. Y. Zhang, and D. Gall, "Epitaxial TiN(001) wetting layer for growth of thin single-crystal Cu(001)," *Journal of Applied Physics*, vol. 110, p. 043714, 2011.
- [8] P. Patsalas, N. Kalfagiannis, S. Kassavetis, G. Abadias, D. V. Bellas, C. Lekka, and E. Lidorikis, "Conductive nitrides: Growth principles, optical and electronic properties, and their perspectives in photonics and plasmonics," *Materials Science and Engineering: R: Reports*, vol. 123, pp. 1-55, January 2018.
- [9] S. Kassavetis, A. Hodroj, C. Metaxa, S. Logothetidis, J. F. Pierson, and P. Patsalas, "Optical and electronic properties of conductive ternary nitrides with rare- or alkaline-earth elements," *Journal of Applied Physics*, vol. 120, p. 225106, 2016.
- [10] S. Kassavetis, D. V. Bellas, G. Abadias, E. Lidorikis, and P. Patsalas, "Plasmonic spectral tunability of conductive ternary nitrides," *Applied Physics Letters*, vol. 108, p. 263110, 2016.
- [11] K. Balasubramanian, S. V. Khare, and D. Gall, "Valence electron concentration as an indicator for mechanical properties in rocksalt structure nitrides, carbides and carbonitrides," *Acta Materialia*, vol. 152, pp. 175-185, June 2018.
- [12] D. Gall, I. Petrov, and J. E. Greene, "Epitaxial Sc1-xTixN(001): Optical and electronic transport properties," *Journal of Applied Physics*, vol. 89, pp. 401-409, 2001.
- [13] D. Gall, M. Stoehr, and J. Greene, "Vibrational modes in epitaxial Ti1-xScxN (001) layers: An ab initio calculation and Raman spectroscopy study," *Physical Review B*, vol. 64, p. 174302, 2001.
- [14] F. Tian, J. D'Arcy-Gall, T.-Y. Lee, M. Sardela, D. Gall, I. Petrov, and J. E. Greene, "Epitaxial Ti1-xWxN alloys grown on MgO(001) by ultrahigh vacuum reactive magnetron sputtering: Electronic properties and long-range cation ordering," *Journal of Vacuum Science & Technology A*, vol. 21, pp. 140-146, 2003.
- [15] B. Saha, J. A. Perez-Taborda, J.-H. Bahk, Y. R. Koh, A. Shakouri, M. Martin-Gonzalez, and T. D. Sands, "Temperature-dependent thermal and thermoelectric properties of n-type and p-type Sc1-xMgxN," *Physical Review B*, vol. 97, p. 085301, February 2018.
- [16] B. Wang, S. Kerdsongpanya, M. E. McGahay, E. Milosevic, P. Patsalas, and D. Gall, "Growth and properties of epitaxial Ti1-xMgxN(001) layers," *Journal of Vacuum Science & Technology A*, vol. 36, p. 061501, September 2018.
- [17] M. Balzer, M. Fenker, H. Kappl, T. Müller, A. Heyn, A. Heiss, and A. Richter, "Corrosion protection of steel substrates by magnetron sputtered TiMgN hard coatings: Structure, mechanical properties and growth defect related salt spray test results," *Surface and Coatings Technology*, vol. 349, pp. 82-92, September 2018.
- [18] A. Hodroj, O. Chaix-Pluchery, P. Steyer, and J. F. Pierson, "Oxidation resistance of decorative (Ti,Mg)N coatings deposited by hybrid cathodic arc evaporation-magnetron sputtering process," *Surface and Coatings Technology*, vol. 205, pp. 4547-4553, 6/25/2011.
- [19] C. Metaxa, S. Kassavetis, J. F. Pierson, D. Gall, and P. Patsalas, "Infrared Plasmonics with Conductive Ternary Nitrides," ACS Applied Materials & Interfaces, vol. 9, pp. 10825-10834, March 2017.
- [20] S. Ishii, R. P. Sugavaneshwar, and T. Nagao, "Titanium Nitride Nanoparticles as Plasmonic Solar Heat Transducers," *The Journal of Physical Chemistry C*, vol. 120, pp. 2343-2348, February 2016.
- [21] M. A. Gharavi, R. Armiento, B. Alling, and P. Eklund, "Theoretical study of phase stability, crystal and electronic structure of MeMgN2 (Me = Ti, Zr, Hf) compounds," *Journal of Materials Science*, November 2017.
- [22] B. Alling, "Metal to semiconductor transition and phase stability of Ti(1-x)Mg(x)Ny alloys investigated by first-principles calculations," *Physical Review B*, vol. 89, p. 085112, February 2014.
- [23] I. Yoshihiro and U. Mamoru, "First-principles calculations of semiconducting TiMgN2," *Japanese Journal of Applied Physics*, vol. 55, p. 098001, 2016.
- [24] N. Finnegan, R. T. Haasch, D. Gall, S. Kodambaka, J. E. Greene, and I. Petrov, "A Comparison of Auger Electron Spectra from Stoichiometric

- Epitaxial TiN(001) After (1) UHV Cleaving and (2) Ar+ Sputter Etching," *Surface Science Spectra*, vol. 7, pp. 93-100, 2000.
- [25] D. K. Smith and H. R. Leider, "Low-temperature thermal expansion of LiH, MgO and CaO," *Journal of Applied Crystallography*, vol. 1, pp. 246-249, 1968.
- [26] M. Fenker, M. Balzer, H. Kappl, and O. Banakh, "Some properties of (Ti,Mg)N thin films deposited by reactive dc magnetron sputtering," Surface and Coatings Technology, vol. 200, pp. 227-231, October 2005.
- [27] C.-S. Shin, S. Rudenja, D. Gall, N. Hellgren, T.-Y. Lee, I. Petrov, and J. E. Greene, "Growth, surface morphology, and electrical resistivity of fully strained substoichiometric epitaxial TiNx (0.67 ≤ x<1.0) layers on MgO(001)," *Journal of Applied Physics*, vol. 95, pp. 356-362, 2004.
- [28] J. A. Sue, "X-ray elastic constants and residual stress of textured titanium nitride coating," in *Metallurgical Coatings and Thin Films* 1992, B. D. Sartwell, G. E. McGuire, and S. Hofmann, Eds., ed Amsterdam: Elsevier, 1992, pp. 154-159.
- [29] K. Zhang, M. Wen, S. Wang, R. P. Deng, D. Gall, and W. T. Zheng, "Sputter deposited NbCxNy films: Effect of nitrogen content on structure and mechanical and tribological properties," *Surface and Coatings Technology*, vol. 258, pp. 746-753, November 2014.
- [30] A. B. Mei, M. Tuteja, D. G. Sangiovanni, R. T. Haasch, A. Rockett, L. Hultman, I. Petrov, and J. E. Greene, "Growth, nanostructure, and optical properties of epitaxial VNx/MgO(001) (0.80 [less-than-or-equal] x [less-than-or-equal] 1.00) layers deposited by reactive magnetron sputtering," *Journal of Materials Chemistry C*, vol. 4, pp. 7924-7938, 2016.
- [31] X. Y. Zhang, J. S. Chawla, B. M. Howe, and D. Gall, "Variable-range hopping conduction in epitaxial CrN(001)," *Physical Review B*, vol. 83, p. 165205, April 2011.
- [32] X. Y. Zhang, J. S. Chawla, R. P. Deng, and D. Gall, "Epitaxial suppression of the metal-insulator transition in CrN," *Physical Review B*, vol. 84, p. 073101, August 2011.
- [33] C.-S. Shin, D. Gall, Y.-W. Kim, P. Desjardins, I. Petrov, J. E. Greene, M. Odén, and L. Hultman, "Epitaxial NaCl structure δ-TaNx(001): Electronic transport properties, elastic modulus, and hardness versus N/Ta ratio," *Journal of Applied Physics*, vol. 90, pp. 2879-2885, 2001.
- [34] C.-S. Shin, D. Gall, P. Desjardins, A. Vailionis, H. Kim, I. Petrov, J. E. Greene, and M. Odén, "Growth and physical properties of epitaxial metastable cubic TaN(001)," *Applied Physics Letters*, vol. 75, pp. 3808-3810, 1999.
- [35] H.-S. Seo, T.-Y. Lee, I. Petrov, J. E. Greene, and D. Gall, "Epitaxial and polycrystalline HfNx (0.8≤x≤1.5) layers on MgO(001): Film growth

- and physical properties," *Journal of Applied Physics*, vol. 97, p. 083521, 2005.
- [36] D. Gall, M. Städele, K. Järrendahl, I. Petrov, P. Desjardins, R. T. Haasch, T. Y. Lee, and J. E. Greene, "Electronic structure of ScN determined using optical spectroscopy, photoemission, and ab initio calculations," *Physical Review B*, vol. 63, p. 125119, March 2001.
- [37] R. Deng, B. D. Ozsdolay, P. Y. Zheng, S. V. Khare, and D. Gall, "Optical and transport measurement and first-principles determination of the ScN band gap," *Physical Review B*, vol. 91, p. 045104, January 2015.
- [38] A. R. Smith, H. A. H. AL-Brithen, D. C. Ingram, and D. Gall, "Molecular beam epitaxy control of the structural, optical, and electronic properties of ScN(001)," *Journal of Applied Physics*, vol. 90, pp. 1809-1816, 2001.
- [39] H. A. Al-Brithen, A. R. Smith, and D. Gall, "Surface and bulk electronic structure of ScN(001) investigated by scanning tunneling microscopy/spectroscopy and optical absorption spectroscopy," *Physical Review B*, vol. 70, p. 045303, July 2004.
- [40] H. Kindlund, D. G. Sangiovanni, J. Lu, J. Jensen, V. Chirita, J. Birch, I. Petrov, J. E. Greene, and L. Hultman, "Vacancy-induced toughening in hard single-crystal V0.5Mo0.5Nx/MgO(001) thin films," *Acta Materialia*, vol. 77, pp. 394-400, September 2014.
- [41] D. Gall, C.-S. Shin, R. T. Haasch, I. Petrov, and J. E. Greene, "Band gap in epitaxial NaCl-structure CrN(001) layers," *Journal of Applied Physics*, vol. 91, pp. 5882-5886, 2002.
- [42] R. Sanjinés, C. Wiemer, J. Almeida, and F. Lévy, "Valence band photoemission study of the Ti-Mo-N system," *Thin Solid Films*, vol. 290, pp. 334-338, December 1996.
- [43] D. Jaeger and J. Patscheider, "A complete and self-consistent evaluation of XPS spectra of TiN," *Journal of Electron Spectroscopy and Related Phenomena*, vol. 185, pp. 523-534, November 2012.
- [44] R. T. Haasch, T.-Y. Lee, D. Gall, J. E. Greene, and I. Petrov, "Epitaxial TiN(001) Grown and Analyzed In situ by XPS and UPS. II. Analysis of Ar+ Sputter Etched Layers," *Surface Science Spectra*, vol. 7, pp. 204-212, 2000.